Molecular Pharmacology Fast Forward. Published on June 12, 2019 as DOI: 10.1124/mol.119.115824
This article has not been copyedited and formatted. The final version may differ from this version.

Generation and characterization of an *Abcc1* humanized mouse model (*hABCC1$^{flx/flx}$*) with knockout capability

Markus Krohn[1,#], Viktoria Zoufal[2], Severin Mairinger[2], Thomas Wanek[2], Kristin Paarmann[1], Thomas Brüning[1], Ivan Eiriz[1], Mirjam Brackhan[1], Oliver Langer[2,3], Jens Pahnke[1,4,5,6,*]

[1] Department of Neuro-/Pathology, University of Oslo (UiO) and Oslo University Hospital (OUS), Oslo, Norway

[2] Biomedical Systems, Center for Health & Bioresources, Austrian Institute of Technology (AIT) GmbH, Seibersdorf, Austria

[3] Department of Clinical Pharmacology and Department of Biomedical Imaging and Image-guided Therapy, Medical University of Vienna (MVU), Vienna, Austria

[4] LIED, University of Lübeck (UzL), Lübeck, Germany

[5] Leibniz-Institute of Plant Biochemistry (IPB), Halle, Germany

[6] Department of Pharmacology, Medical Faculty, University of Latvia (LU), Rīga, Latvia

* J.P. at the University of Oslo, Department of Neuro-/Pathology, Postboks 4950 Nydalen, 0424 Oslo, Norway, Email: jens.pahnke@gmail.com, Tel: +47 230 74166

current address:
University of Lübeck, Institute for Experimental and Clinical Pharmacology and Toxicology, Center of Brain, Behavior and Metabolism (CBBM), Lübeck, Germany

Molecular Pharmacology Fast Forward. Published on June 12, 2019 as DOI: 10.1124/mol.119.115824
This article has not been copyedited and formatted. The final version may differ from this version.

Table of Contents/Abstract Graphics

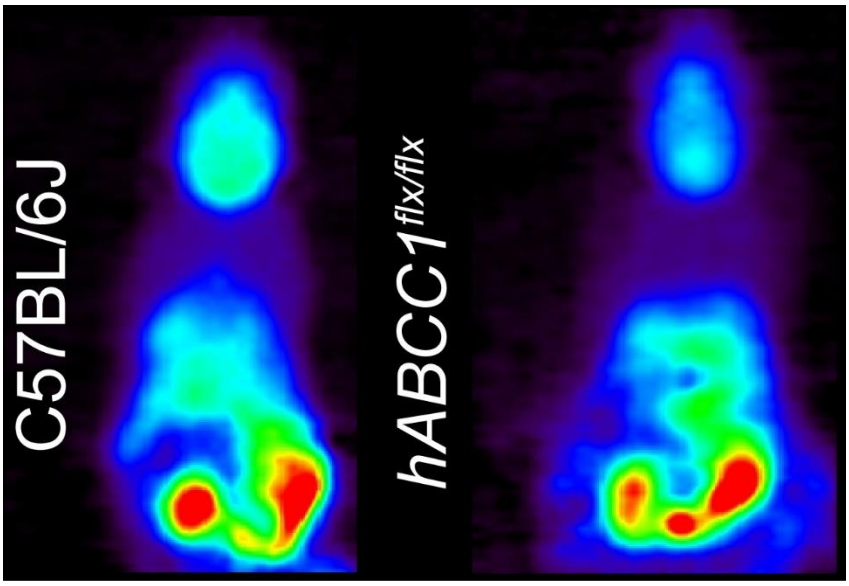

Molecular Pharmacology Fast Forward. Published on June 12, 2019 as DOI: 10.1124/mol.119.115824
This article has not been copyedited and formatted. The final version may differ from this version.

Abstract

ATP-binding cassette transporters such as ABCB1 (P-gp), ABCC1 (MRP1) and ABCG2 (BCRP) are well known for their role in rendering cancer cells resistant to chemotherapy. Additionally, recent research provided evidence that, along with other ABC transporters (ABCA1, ABCA7), they might be cornerstones to tackle neurodegenerative diseases. Overcoming chemoresistance in cancer, understanding drug-drug interactions and developing efficient and specific drugs that alter ABC transporter function are hindered by a lack of *in vivo* research models, which are fully predictive for humans. Hence, the humanization of ABC transporters in mice has become a major focus in pharmaceutical and neurodegenerative research. Here, we present a characterization of the first *Abcc1* humanized mouse line. In order to preserve endogenous expression profiles, we chose to generate a knock-in that leads to the expression of a chimeric protein that is fully human except for one amino acid. We found robust mRNA and protein expression within all major organs analyzed (brain, lung, spleen and kidney). Furthermore, we demonstrate the functionality of the expressed human ABCC1 protein in brain and lungs using functional positron emission tomography (PET) imaging *in vivo*. Through the introduction of loxP sites, we additionally enabled this humanized mouse model for highly sophisticated studies involving cell-type specific transporter ablation. Based on our data, the presented mouse model appears to be a promising tool for the investigation of cell-specific ABCC1 function. It can provide a new basis for better translation of pre-clinical research.

Keywords: ABCC1, MRP1, humanization, PET, drug resistance, ABC transporter

Molecular Pharmacology Fast Forward. Published on June 12, 2019 as DOI: 10.1124/mol.119.115824
This article has not been copyedited and formatted. The final version may differ from this version.

Introduction

ATP-binding-cassette (ABC) transporters play a pivotal role in the protection of the human body against xenobiotics, as mediators in signaling pathways and are crucial to certain metabolic processes (Theodoulou and Kerr, 2015). The probably best characterized ABC transporter is ABCB1 (P-gp). It is highly investigated because of its profound impact on the therapy outcome of many different types of cancer, as is ABCG2 (BCRP) (Noguchi et al., 2014; Wijaya et al., 2017). Both transporters are also significantly contributing to the absorption, distribution, metabolism, and excretion (ADME) of drugs (International Transporter et al., 2010). Due to mostly basolateral cellular localization, ABCC1 is relevant for the body distribution of drugs, but not for their absorption and excretion (International Transporter et al., 2010). Nevertheless, ABCC1 does also play a role in the chemoresistance of different cancers. High ABCC1 expression is, for instance, a negative prognostic factor in cases of soft tissue sarcoma (Citti et al., 2012; Martin-Broto et al., 2014) and both acute myeloid and lymphoblastic leukemia (Liu et al., 2018; van der Kolk et al., 2000; Winter et al., 2013). Such correlation has furthermore been shown for neuroblastoma patients. However, it mainly arises through MYCN gene multiplication and its regulatory connection to ABCC1 (Alisi et al., 2013; Haber et al., 2006). ABCC1 was also found to be the most prominent multi-drug resistance transporter in glioblastoma cells and glioblastoma stem-like cells, which are assumed to be the major reason for the high recurrence rate of glioblastomas (Crowder et al., 2014; Huang et al., 2010; Peignan et al., 2011; Torres et al., 2016). Accordingly, inhibition of ABCC1 was suggested to improve response to glioblastoma-directed chemotherapy (Peignan et al., 2011; Tivnan et al., 2015). Among the known substrates of ABCC1 are drugs like vincristine and etoposide (used in glioblastoma therapy) (Tivnan et al., 2015), methotrexate (psoriasis and cancer treatment), citalopram (treatment of major depression), montelukast (asthma medication) and anthracyclines (treatment of several different classes of cancer) (Chihara et al., 2016; Giordano et al., 2012; McGowan et al., 2017; Nabhan et al., 2015; Smith et al., 2010). It is, however, important to note that ABCC1 is not the main treatment target or mechanism of resistance in many of these conditions. Moreover, a range of endogenously produced molecules like leukotriene C4 (LTC_4)(Leier et al., 1994), 17β-estradiol 17-(β-D-glucuronide) ($E_2$17βG) (Stride et al., 1997), sphingosine-1-phosphate (S1P) (Cartwright et al., 2013) and Cobalamin (vitamin B12) (Beedholm-Ebsen et al., 2010) as well as glutathione, glucuronide, and sulfate conjugates (Jedlitschky et al., 1996; Muller et al., 1994) require ABCC1 for their extrusion and/or relocation. Furthermore, our own work provided evidence that ABCC1 function is of important relevance with regard to Alzheimer's disease (Hofrichter et al., 2013; Krohn et al., 2015; Krohn et al., 2011), and in sustaining the homeostasis of neural stem and progenitor cells (NSPCs) in healthy and diseased mouse brains (Pahnke et al., 2013; Schumacher et al., 2012). Recently, a family with clinical fronto-temporal

Molecular Pharmacology Fast Forward. Published on June 12, 2019 as DOI: 10.1124/mol.119.115824
This article has not been copyedited and formatted. The final version may differ from this version.

dementia/degeneration (FTD), but autopsy-confirmed histological AD, has been discovered in the United States to have a germline mutation in the *ABCC1* gene (chr16:16216007 A>G, p.Y1189C) (unpublished data).

As is known for ABCB1 and ABCG2, the substrate specificity of the murine ABCC1 protein differs from that of its human orthologue. For example, Stride and colleagues have shown that both human and mouse ABCC1 transporters have similar affinities to LTC_4, vinblastine, vincristine and VP-16 (Stride et al., 1997). However, the murine ABCC1 was found to be incapable of transporting any of the anthracyclines tested (doxorubicin, epirubicin, daunorubicin) (Stride et al., 1997). In a mutagenesis study, the group was later able to determine that a single amino acid (E1089, human protein) is important for conferring the anthracycline resistance (Zhang et al., 2001). Conversely, the reciprocal mutation Q1086E in the mouse orthologue led to only about 60% of the resistance level of the human ABCC1 expressing cell line (Zhang et al., 2001). Stride *et al.* also found that the endogenous metabolite $E_2$17βG is efficiently transported by human ABCC1, but far less by the mouse orthologue (Stride et al., 1997).

In light of the known and further expected differences between human and mouse ABC transporter substrate specificities, the establishment of mouse models that express the human transporter instead of their endogenous orthologue is being pursued (Choo and Salphati, 2018). This so-called humanization of mice holds the promise of bridging cross-species differences during pre-clinical drug development and increasing the clinical relevance of results obtained from mouse models of various diseases (Devoy et al., 2011).

Because of its impact on the outcome of various therapies, disease development and the described differences between mouse and human ABCC1 protein substrate specificities, we sought to establish an *Abcc1* humanized mouse model. In the present work, we describe the generation and basic characterization of a mouse model that expresses the mouse-human chimeric *ABCC1* gene (>99.9% human) under the endogenous *Abcc1* promoter. We determined mRNA and protein expression levels in multiple organs and verified ABCC1 function *in vivo* using positron emission tomography (PET) imaging.

Methods

Generation of humanized ABCC1 mice (*hABCC1*$^{flx/flx}$)

Model design and generation was performed by and in collaboration with genOway (Lyon, France).

Molecular Pharmacology Fast Forward. Published on June 12, 2019 as DOI: 10.1124/mol.119.115824
This article has not been copyedited and formatted. The final version may differ from this version.

Targeting vector construct

Humanization of the murine *Abcc1* gene was performed by in-frame replacement of exon 2 with the human *ABCC1* coding sequence (CDS, devoid of the first exon) to keep it under control of the endogenous promoter. Downstream of the *hABCC1* CDS a Neomycin resistance cassette (flanked by FRT sites for later Flp-mediated excision) was introduced to enable positive selection of clones (Figure 1). Moreover, the CDS was flanked by loxP sites to allow Cre-recombinase mediated deletion. Since deletion of the human CDS would result in restoration of the murine *Abcc1* gene and protein expression (lacking only exon 2 encoded amino acids), additionally two point mutations in exon 3 of the murine gene were inserted. With these mutations, premature STOP codons are present in each of the three possible reading frames.

Generation and screening of humanized ABCC1 ES cell clones

The linearized targeting vector with a size of 19 kbp was purified and used for electroporation of C57BL/6N embryonic stem (ES) cells according to genOway's standard electroporation procedure ($5x10^6$ ES cells in the presence of 40 µg vector, 260 Volt, 500 µF). Positive selection was initiated after 48 h using 200 µg/ml G418 (Sigma-Aldrich). The electroporation session resulted in 144 positive clones which were amplified as duplicates in 96 well plates. One set of clones was frozen and stored at -80 °C. The second set of clones was used for DNA preparation and screened for homologues recombination (HR). After initial PCR screening for the HR event, amplificates of correct size were sequenced to confirm integrity of the transgene and presence of the two point mutations in exon 3. Out of eleven ES cell clones picked for sequencing, 9 clones were confirmed to be flawless. Southern blots furthermore confirmed correct integration of the 3' and 5' ends of the vector in six of these clones.

Generation of chimeric mice and breeding

In order to generate chimeric mice, recipient blastocysts were isolated from B6(Cg)-Tyr^{c-2J}/J mice. For injection into blastocysts, 4 ES cell clones were selected which were re-implanted into pseudo-pregnant OF1 females. The B6(Cg)-Tyr^{c-2J}/J mice carry a mutation causing albinism but are otherwise genetically identical with C57BL/6J mice. This mutation allows easy monitoring of the degree of chimerism of the offspring generated by the combination of blastocysts from white-colored mice and ES cell clones from black-colored mice. 6 males from 3 different clones with more than 50% chimerism were generated and used for breeding with C57BL/6J Flp deleter mice as soon as animals reached sexual maturity. Breeding to Flp deleter mice ensured excision of the neomycin cassette as well as restoration of uniform black fur color. Only in chimeras from one ES cell clone germline transmission was observed resulting in 12 F1 animals. Only two males were found to be lacking the neomycin resistance cassette. After positive re-evaluation of transgene integration by Southern blot, these males were bred to C57BL/6J females to

Molecular Pharmacology Fast Forward. Published on June 12, 2019 as DOI: 10.1124/mol.119.115824
This article has not been copyedited and formatted. The final version may differ from this version.

establish the *hABCC1*$^{flx/flx}$ mouse line. The *hABCC1*$^{flx/flx}$ mice were registered in the Mouse Genome Informatics (MGI) database as B6.Cg-Abcc1$^{tm1.1(ABCC1)Pahnk}$ (MGI:6258225).

Genotyping

To guide and control breeding of the *hABCC1*$^{flx/flx}$ and *hABCC1*$^{-/-}$ animals, we designed a 3-primer-PCR able to distinguish all 6 possible genotypes (wt/wt; wt/fl; flx/flx; 0/fl; wt/0; -/-). To do so, we exploited a 67 bp inset introduced upstream of exon 2 that contains the 5'-loxP site and 35 additional non-endogenous nucleotides. As this sequence is only present in *Abcc1* modified mice, a two-primer-PCR can distinguish between wild-type *Abcc1* and *hABCC1*$^{flx/flx}$ alleles. A third (reverse) primer was placed downstream of the 3'-loxP side that produces a band only when the *hABCC1* CDS was excised. Primers used were N351_humC1_common (5'- cacatagtcctggcatttgg), N352_humC1_rc (5'- taagatggagggaggctgtc) and N353_humC1_rcCre (5'- tctcaagttccaggtcagcc). Band patterns produced by the different genotypes are summarized in Supplementary Table 1. PCR cycling was run as follows: 5 min @ 95 °C, 35 cycles of 45 s @ 95 °C, 60 s @ 62 °C and 90 s @ 72 °C followed by 5 min @ 72 °C.

Additional mouse models

C57BL/6J wild-type and Cre-deleter (B6.C-Tg(CMV-cre)1Cgn/J, JAX:006054) mice were purchased from The Jackson Laboratory (Bar Harbor, USA). To induce *hABCC1* knockout, we crossbred *hABCC1*$^{flx/flx}$ mice to Cre-deleter mice. The resulting homozygous knockout mice are referred to as *hABCC1*$^{-/-}$ mice and were registered as B6.Cg-Abcc1$^{tm1.2Pahnk}$ (MGI:6258262) in the Mouse Genome Informatics (MGI) database. Conventional *Abcc1* knockout mice (FVB.129P2-Abcc1^{tm1Bor} N12 (Taconic Farms, Denmark)) (Wijnholds et al., 1997) were backcrossed to C57BL/6J mice for more than 12 generations to produce *Abcc1*$^{-/-}$ mice within the same genomic background as *hABCC1*$^{flx/flx}$ and *hABCC1*$^{-/-}$ mice. All strains were bred and housed under SOPF conditions at 21±1 °C, 12 h/12 h light/dark cycle with food (PM3, Special Diet Services) and acidified water *ad libitum*. All protocols involving the breeding and use of animals were approved by the Norwegian Food Safety (Mattilsynet) and the Austrian authorities (Amt der Niederösterreichischen Landesregierung). All study procedures were performed in accordance with the European Communities Council Directive of September 22, 2010 (2010/63/EU).

Tissue Preparation

Mice were sacrificed by cervical dislocation. After quick intracardial perfusion with 10 ml ice-cold PBS one hemisphere of each brain was snap-frozen in liquid nitrogen within 3 min after death. Additionally,

Molecular Pharmacology Fast Forward. Published on June 12, 2019 as DOI: 10.1124/mol.119.115824
This article has not been copyedited and formatted. The final version may differ from this version.

samples of lung, spleen and kidney were taken and snap frozen. All snap-frozen samples were stored at -80 °C until use.

Quantitative PCR

Tissue samples of 100-days-old wild-type (4 female, 1 male), *hABCC1*$^{flx/flx}$ (4 male) and *hABCC1*$^{-/-}$ (4 female, 1 male) mice were thawed on ice in RNAlater® (Life Technologies, USA) and homogenized using ceramic beads (SpeedMill PLUS, analyticjena AG, Germany). Total RNA of about 25 mg tissue was isolated using TRIzol (Life Technologies, USA) and gene expression analyzed employing EXPRESS One-Step qPCR SuperMIX (Life Technologies, USA). Primer sets with respective TaqMan® probes for mouse *Abcc1* (Mm00456156_m1), human *ABCC1* (Hs01561504_m1) and mouse *Actb* (Mm00607939_s1) genes were purchased from Thermo Fisher Scientific Inc. (USA). TaqMan® assays are sets of primers and a probe validated for similar amplification efficiencies between different assays to ensure comparability. VIC labelled *Actb* Assays were run together with FAM labelled *Abcc1* and *ABCC1* assays, respectively, in the same tubes to allow normalization of gene expression and calculation of $\Delta\Delta C_t$ values. All samples were tested with each TaqMan Assay, including a non-template control. Reactions were performed according to manufacturer's instructions with a final volume of 20 µl and 75 ng of RNA. PCR amplification was performed using an AriaMX (Agilent Technologies), conditions were 15 min @ 50 °C, 2 min @ 95 °C followed by 40 cycles of 15 s @ 95 °C and 1 min @ 60 °C.

Western blot

Brain hemispheres of 100-days-old wild-type (5 females, 6 males), *hABCC1*$^{flx/flx}$ (6 females, 5 males) and *hABCC1*$^{-/-}$ (6 females, 5 males) mice were thawed on ice in RNAlater® (Life Technologies, USA) and Choroid plexuses (CP) were separated from the lateral ventricle using a preparative microscope. Each CP was put into 20 µl of membrane protein lysis buffer (100 mM Tris pH 8, 20 mM EDTA, 140 mM NaCl, 5 % SDS and protease inhibitors (cOmplete™ mini tablets, Roche)) and incubated for 1 h @ 50 °C with occasional up-and-down pipetting. The remaining brain tissue as well as spleen, lung and kidney samples were bead-homogenized. About 25 mg homogenate was taken for protein extraction using lysis buffer A (100 mM Tris pH 7.4, 150 mM NaCl, 0.1 % TritonX-100, DNase I and protease inhibitors (cOmplete™ mini tablets, Roche)). Samples were again submitted to bead homogenization and incubated 15 min at room temperature before centrifugation at 4 °C (13,000 rpm, 90 min). The pellets were resuspended in membrane protein lysis buffer and samples incubated at 50 °C for 1 h before another round of centrifugation (RT, 13.000 rpm, 30 min). Supernatants were collected and subjected to protein concentration determination using a BCA assay kit (Pierce, ThermoFisher Scientific, USA). For Western

Molecular Pharmacology Fast Forward. Published on June 12, 2019 as DOI: 10.1124/mol.119.115824
This article has not been copyedited and formatted. The final version may differ from this version.

blotting, samples were prepared with Laemmli buffer and subjected to gel electrophoresis using a 7.5 % TGX self-casted gel matrix (Bio-Rad, Germany) and 60 µg protein per lane. In case of CP samples, half the available volume per sample (about 13 µl) was used per lane without determination of protein concentration due to the limited sample volume. Proteins were blotted onto 0.22 µm PVDF membranes using a Trans-Blot Turbo system (Bio-Rad, Germany) and membranes blocked with 1.5 % non-fat dry milk in PBS-0.01 % Tween20 for 1 h at room temperature. For protein detection, anti-ABCC1 antibody MRPr1 (1:400, ab3368, Abcam), QCRL-1 (1:100, sc-18835, SantaCruz) and IU2H10 (1:100, ab32574, Abcam) were used and incubated overnight at 4 °C. anti-ATP1A2 antibody (EPR11896(B)) (ab166888, Abcam, 1:2,000) was used to assess amounts of NaCl-ATPase serving as endogenous control. Secondary antibodies used for detection were HRP-conjugated, anti-rat (112-035-167, Jackson ImmunoResearch; 1:10,000), three different anti-mouse antibodies to exclude secondary antibody related detection issues ((sc-516102, SantaCruz, 1:1,000), (NB720H, Novus Biologicals, 1:2,000 (A90-216P, Bethyl Laboratories, 1:5,000)), and anti-rabbit (711-035-152, Jackson ImmunoResearch; 1:10,000) antibodies, incubated for 1 h at room temperature in PBS-0.01 % Tween20. After washing, Clarity-plus (Bio-Rad, Germany) ECL detection reagent was distributed over the PVDF membranes and light signals were detected using the Octoplus QPLEX system (DyeAGNOSTICS, Germany). Signal analysis was performed using Image Studio Lite (LI-COR) and Microsoft Excel (Office365).

Positron emission tomography (PET) imaging

Imaging experiments were performed under isoflurane anesthesia. Animals (all females) were warmed throughout the experiment and body temperature and respiratory rate were constantly monitored. Mice were placed in a custom-made imaging chamber and the lateral tail vein was cannulated for *i.v.* administration. A microPET Focus220 scanner (Siemens Medical Solutions, Knoxville, TN, USA) was used for PET imaging. Mice were *i.p.* injected under anesthesia at 30 min before start of the PET scan either with vehicle solution (phosphate-buffered saline, PBS; wild-type: n = 6, *hABCC1*$^{flx/flx}$: n = 5, *hABCC1*$^{-/-}$: n = 4, *Abcc1*$^{-/-}$: n = 6), or with MK571 (CAS Number: 115103-85-0, 300 mg/kg; *hABCC1*$^{flx/flx}$: n = 3, wild-type: n = 7). Subsequently, 6-bromo-7- [^{11}C]methylpurine (32.85 ± 7.34 MBq; 0.1 ml; 1.26 ± 14.80 nmol) which had been synthesized as described previously (Zoufal et al., 2019) was administered as an *i.v.* bolus via the lateral tail vein and a 90-min dynamic PET scan was initiated at the start of radiotracer injection (timing window 6 ns; energy window of 250-750 keV).

The PET data were sorted into 25 frames with a duration increasing from 5 s to 20 min. PET images were reconstructed using Fourier re-binning of the 3-dimensional sinograms followed by a 2-dimensional filtered back-projection with a ramp filter giving a voxel size of 0.4 × 0.4 × 0.796 mm³. Using AMIDE

Molecular Pharmacology Fast Forward. Published on June 12, 2019 as DOI: 10.1124/mol.119.115824
This article has not been copyedited and formatted. The final version may differ from this version.

software (Loening and Gambhir, 2003), whole brain and right lung were manually outlined on the PET images to derive concentration-time curves expressed in units of standardized uptake value (SUV = (radioactivity per g/ injected radioactivity) × body weight). From the log-transformed concentration-time curves the elimination slope of radioactivity washout from tissue ($k_{elimination,brain}$ or $k_{elimination,lung}$, h^{-1}) was determined by linear regression analysis of data from 17.5 to 80 min after radiotracer injection (Zoufal et al., 2019).

Statistics

This study is exploratory in nature. Thus, all p-values are descriptive only. Data were analyzed using Microsoft Excel 365 and GraphPad Prism 8.0 using the statistical tests indicated in the figure legends. All reported values are means and error bars indicate standard deviation.

Results

Design and generation of *hABCC1$^{flx/flx}$* mice

Earlier publications indicate that promoter elements driving *Abcc1* expression in mice and rats are primarily located from position -27bp and upstream (relative to the TSS) (Kurz et al., 2001; Muredda et al., 2003). However, more recent data from DNase-seq and ATAC-seq experiments indicate regulatory relevance of the first exon and segments within the first intron around +10kbp and +16kbp (ENCODE datasets ENCSR791AJY and ENCSR310MLB, Supplementary Fig. 1). Furthermore, in-house analysis performed by genOway indicated DNase I protected sites and transcription factor (TF) binding sites in the 5' region of the *Abcc1* gene (Figure 2).

To conserve these structures and avoid dysfunctional integration as in case of *Abcb1* humanized mice (Krohn et al., 2018), we decided to introduce the human *ABCC1* CDS in-frame into mouse exon 2, which is devoid of potential regulatory elements. We thereby generated a chimeric mouse/human *ABCC1* gene (Figure 1). However, the first exon of both genes encodes 16 amino acids with only one amino acid being different (human: 1MALR**G** FCSAD GSDPL W16; mouse: 1MALR**S** FCSAD GSDPL W16). This strategy can be expected to result in some re-expression of *Abcc1* mRNA after recombination of the hABCC1flx/flx locus via Cre recombinase. Since the 5'-UTR and exon 1 are left untouched, transcription of the re-combined gene will still be initiated producing an mRNA lacking exon 2 (Δex2-*Abcc1*). Although not recognized by the RNA polymerase, the additional stop codons we introduced in exon 3 should effectively terminate translation of this Δex2-*Abcc1* mRNA into proteins.

Molecular Pharmacology Fast Forward. Published on June 12, 2019 as DOI: 10.1124/mol.119.115824
This article has not been copyedited and formatted. The final version may differ from this version.

ABCC1 expression

To assess the functionality of the new mouse lines, we determined mRNA and protein expression of murine *Abcc1* and human *ABCC1* in 100-days-old, wild-type, *hABCC1*$^{flx/flx}$ and *hABCC1*$^{-/-}$ mice. As expected, the TaqMan assay for human *ABCC1* mRNA neither generated signals in wild-type mice nor in *hABCC1*$^{-/-}$ mice indicating the species specificity of the assay and, more importantly, successful *ABCC1* knockout in *hABCC1*$^{-/-}$ mice (Supplementary Figure 1). In *hABCC1*$^{flx/flx}$ mice, *ABCC1* mRNA was expressed in the brain, but at significantly lower levels than wild-type mRNA ($p=0.0005$) while significantly stronger expression was found in lung tissues ($p<0.0001$). Murine *Abcc1* mRNA, however, was hardly detectable in brain ($p=0.0003$) and not detectable in the lungs of *hABCC1*$^{flx/flx}$ animals (Supplementary Figure 1). Nevertheless, mRNA is not a reliable predictor of protein abundance or function (de Sousa Abreu et al., 2009; Maier et al., 2009; Pascal et al., 2008; Vogel and Marcotte, 2012).

Hence, we sought to determine ABCC1 protein expression in the newly developed mouse strains. hABCC1 protein abundance was determined by Western blotting of whole brain homogenates from *hABCC1*$^{flx/flx}$ mice and revealed an about 60 % higher ($p=0.0002$) ABCC1 abundance than in wild-type mouse brains (Figure 3A, C). In lung tissue, we found robust ABCC1 expression in *hABCC1*$^{flx/flx}$ mice that was comparable to the expression in wild-type mice (Figure 4 B, C). In both tissues, no detectable amounts of ABCC1 were found in *hABCC1*$^{-/-}$ animals, indicating that the introduced stop-codons are recognized by the translation machinery and interrupt the expression of any residual *Abcc1* gene product (Figure 4). The same pattern of expression was found in Western blots of kidney and spleen (Supplementary Fig. 2). We also analyzed single CPs from lateral ventricles, because the CP is the primary location of ABCC1 expression in the brain. As determination of the protein concentration was not possible with such minute amounts of tissue and the extraction of the whole CP was not successful in all cases, the amounts of protein per lane varied substantially. Nevertheless, the signals indicated a similar relative expression between the groups as we have found in the other organs (Supplementary Figure 2). In order to account for a likely higher binding affinity to human than mouse ABCC1 proteins (Hipfner et al., 1998) of the used MRPr1 antibody clone, we sought to use an antibody that recognizes a common epitope. The antibody clone IU2H10 was found to bind to amino acids 8 to 17 and should thus show the same affinity in both species (Chen et al., 2002). Unexpectedly, using this antibody did not result in detection of any band, regardless of the protocol used (data not shown). To further verify that only hABCC1 proteins are expressed in *hABCC1*$^{flx/flx}$ mice, we used the QCRL-1 antibody clone (Hipfner et al., 1998) which is reported to <u>not</u> recognize mouse ABCC1. However, in our hands this antibody recognized an unknown protein of about the same size as ABCC1. As shown in Supplementary Fig. 3, all

Molecular Pharmacology Fast Forward. Published on June 12, 2019 as DOI: 10.1124/mol.119.115824
This article has not been copyedited and formatted. The final version may differ from this version.

samples, including wild-type brains, show the same band pattern. As additional control, we also blotted samples prepared from the well characterized conventional *Abcc1*$^{-/-}$ mice (Wijnholds et al., 1997), which also showed a positive staining (Supplementary Fig. 3). Hence, using these antibodies did not yield any further results.

Positron emission tomography (PET) imaging

The most important physiologic readout of any transgenic model is protein function. We used PET together with 6-bromo-7-[^{11}C]methylpurine to measure ABCC1 transport activity *in vivo*. After *i.v.* injection, 6-bromo-7-[^{11}C]methylpurine is distributed throughout the body, presumably by passive diffusion, and conjugated to glutathione within the cells by glutathione-*S*-transferases. The resulting metabolite S-(6-(7-[^{11}C]methylpurinyl))glutathione is eliminated from tissue by ABCC1. 6-bromo-7-[^{11}C]methylpurine has been used before to measure ABCC1 transport activity in the brain and lungs of mice (Okamura et al., 2009; Okamura et al., 2013).

By means of 6-bromo-7-[^{11}C]methylpurine PET we compared ABCC1 transport activity in wild-type, *hABCC1*$^{flx/flx}$, *hABCC1*$^{-/-}$ and *Abcc1*$^{-/-}$ mice to verify transporter functionality in the humanized mouse model. To further assess transporter function we also acquired 6-bromo-7-[^{11}C]methylpurine PET scans in wild-type and *hABCC1*$^{flx/flx}$ mice after pre-treatment with the ABCC1 inhibitor MK571 (300 mg/kg, i.p.). In Figure 5, representative PET images of all groups are depicted. No visual differences in radioactivity distribution to the brains and lungs could be observed between *hABCC1*$^{flx/flx}$ and wild-type mice. In both *hABCC1*$^{-/-}$ mice and *Abcc1*$^{-/-}$ mice radioactivity uptake in the brain and lungs was higher than in *hABCC1*$^{flx/flx}$ and wild-type mice. After MK571 pre-treatment, radioactivity uptake in brain and lungs of *hABCC1*$^{flx/flx}$ and wild-type mice was increased relative to vehicle-treated animals (Figure 5). Concentration-time curves of radioactivity in the brain and lungs of all investigated mouse groups are shown in Figure 6A-D. As an outcome parameter of ABCC1 function, we determined the slope of radioactivity elimination from tissue ($k_{elimination,brain}$ and $k_{elimination,lung}$, h^{-1}) (Figure 6E, F). $K_{elimination,brain}$ of *hABCC1*$^{flx/flx}$ mice exceeded that of wild-type mice by 43% ($k_{elimination,brain,}$ *hABCC1*$^{flx/flx}$: 1.96 ± 0.1 h^{-1}, wild-type: 1.37 ± 0.27 h^{-1}), while *hABCC1*$^{-/-}$ and *Abcc1*$^{-/-}$ mice were characterized by an almost complete loss of radioactivity washout ($k_{elimination,brain}$ *ABCC1*$^{-/-}$: 0.18 ± 0.01 h^{-1}, *Abcc1*$^{-/-}$: 0.15 ± 0.01 h^{-1}) (Figure 6E). $K_{elimination,lung}$ was not significantly different between wild-type and *hABCC1*$^{flx/flx}$ mice with a tendency for higher values in *hABCC1*$^{flx/flx}$ mice ($k_{elimination,lung}$, *hABCC1*$^{flx/flx}$: 1.77 ± 0.17 h^{-1}, wild-type: 1.52 ± 0.1 h^{-1}; Figure 6F). Again, *hABCC1*$^{-/-}$ and *Abcc1*$^{-/-}$ mice were characterized by a virtual lack of radioactivity washout ($k_{elimination,lung}$ *hABCC1*$^{-/-}$: 0.22 ± 0.02 h^{-1}, *Abcc1*$^{-/-}$: 0.26 ± 0.06 h^{-1}) (Figure 6F). Pre-treatment with

Molecular Pharmacology Fast Forward. Published on June 12, 2019 as DOI: 10.1124/mol.119.115824
This article has not been copyedited and formatted. The final version may differ from this version.

MK571 significantly reduced $k_{elimination,brain}$ and $k_{elimination,lung}$ values both in *hABCC1*$^{flx/flx}$ and in wild-type mice (Figure 6E,F).

Discussion

The ABCC1 protein has been described as a "multitasking" transporter by Susan P.C. Cole (Cole, 2014). Considering its diverse functions and diversity of substrates this is certainly a most appropriate description. In the study presented here, we have engineered the to our knowledge first mouse model that expresses the human ABCC1 transporter under the endogenous mouse promoter. An optimal humanized mouse strain would be characterized by 3 major properties: i) the lack of expression of the replaced protein, ii) abundance and activity of the human protein at levels that are similar to the eradicated endogenous one and iii) a tissue distribution of the human protein that resembles the former expression pattern of the endogenous protein. As can be seen in previous *Abcb1a/b* humanization attempts, careful examination of gene- and promoter structures of the endogenous gene is essential to achieve these properties. In 2015, Sadiq *et al.* published the characterization of an *Abcb1a/b* humanized mouse line developed by Taconic (Germany) (Sadiq et al., 2015). Their report clearly showed that this mouse model was not functional concerning human ABCB1 expression and function. In a study published in 2018 by our group, we characterized another *Abcb1a/b* humanized mouse line, developed by genOway (France), which again showed no significant hABCB1 protein expression (Krohn et al., 2018). Very recently, Yamasaki *et al*. published results of the yet last *Abcb1a/b* humanization attempt. They produced a mouse artificial chromosome (MAC) containing the full 210 kb human genomic *ABCB1* locus and generated transchromosomic mice. Despite lacking expression in intestinal epithelia, their analyses indicated functional expression of human ABCB1 at the blood-brain barrier (Yamasaki et al., 2018).

To reduce the risk of deteriorating the *Abcc1* promoter, we decided to pursue a strategy that leads to the expression of a chimeric gene. The chimerism is restricted to the first exon of the gene and results in the difference of a single amino acid at position 5 (G5S). We are not aware of any indication that the very N-terminal amino acids of ABCC1, nor any other ABC transporter, are of relevance to its function or substrate specificity. The first glycosylation site has been described at position N19 by Hipfner *et al.* (Hipfner et al., 1997). In our hands, the ABCC1 protein bands have an observed size of about 175 kDa although mouse and human ABCC1 have a molecular weight of about 190 kDa, which could hint to a lack of glycosylation of the protein. This inconsistency is, however, most likely a technical anomaly because the size of detected ABCC1 in *hABCC1*$^{flx/flx}$ mice is the same as that in wild-type mice, excluding differences in the translation or posttranslational processing of both variants. Leslie *et al.* found in a cysteine substitution study that only a C43S substitution led to a change in arsenide and vincristine

Molecular Pharmacology Fast Forward. Published on June 12, 2019 as DOI: 10.1124/mol.119.115824
This article has not been copyedited and formatted. The final version may differ from this version.

resistance, but no other cysteine exchange within the first 210 amino acids (Leslie et al., 2003). Lastly, deletion of the N-terminus up to amino acid 64 did not alter LTC_4 transport kinetics in a mutation-study by Gao and colleagues (Gao et al., 1998). Hence, we assume that the ABCC1 protein expressed by this *hABCC1*$^{flx/flx}$ mouse line displays transport characteristics identical to fully human ABCC1.

Our mRNA expression analyses revealed substantial differences between wild-type *Abcc1* and *ABCC1* gene transcription in the brain and lungs. In the brain, *ABCC1* expression was significantly lower than wild-type *Abcc1* expression whereas in lungs *ABCC1* mRNA levels were much higher than in wild-type mice. Interestingly, we found marginal restoration of *Abcc1* transcription in *hABCC1*$^{-/-}$ brains while it remained undetectable in lung tissue. Because we were aware that *Abcc1* expression could be restored after Cre-recombination, we introduced additional stop-codons into exon 3 to prevent mRNA translation and expression of a shortened mABCC1 protein. However, the differential effects seen in both tissues might hint towards differing promoter structures being utilized for *Abcc1* transcription in brain versus lung tissue. Since mRNA expression levels show a generally poor correlation with protein expression, mRNA expression analyses alone can be rather misleading (de Sousa Abreu et al., 2009; Maier et al., 2009; Pascal et al., 2008; Vogel and Marcotte, 2012).

Hence, we employed Western blotting to verify protein expression in brain and lung tissues as well as in spleen, kidney and CP. In contrast to the mRNA results, immunoblotting data revealed protein expression levels in *hABCC1*$^{flx/flx}$ mice that were mostly similar to wild-type animals. In *hABCC1*$^{flx/flx}$ brain tissue, however, the ABCC1 expression was higher than in wild-type brains despite lower *ABCC1* mRNA expression in *hABCC1*$^{flx/flx}$ mice. It should be noted that currently no commercially available anti-ABCC1 antibody can differentiate between mABCC1 and hABCC1 proteins. The used MRPr1 antibody clone recognizes a common epitope between G238 and E247 (human numbering). However, in mABCC1 a serine is found at position 238 instead of a glycine, likely leading to a lower affinity of the MRPr1 antibody to the mABCC1 protein. It is likely, that hABCC1 expression determined using this antibody overestimates the actual protein expression. To account for this difference and further prove absence of any mABCC1 protein in *hABCC1*$^{flx/flx}$ mice, we intended to use the IU2H10 and QCRL-1 antibodies, respectively. Regrettably, despite using different protocols and production batches, none of these antibodies yielded further insights. In our mouse brain samples, the IU2H10 did not give any signal at all and the QCRL-1 antibody bound to an unknown protein even in the extensively used and characterized conventional *Abcc1*$^{-/-}$ mice developed by Wijnholds et al. (Wijnholds et al., 1997). Nevertheless, our data generated from *hABCC1*$^{-/-}$ mice using the MRPr1 antibody clearly indicate, that after Cre-recombination neither human nor mouse ABCC1 proteins are expressed. Although highly unlikely, translation of *Abcc1* mRNA expressed in *hABCC1*$^{flx/flx}$ and *hABCC1*$^{-/-}$ mice could be initiated within exon 8 (first possible in-

Molecular Pharmacology Fast Forward. Published on June 12, 2019 as DOI: 10.1124/mol.119.115824
This article has not been copyedited and formatted. The final version may differ from this version.

frame ATG codon after exon 3 producing a protein not detected by MRPr1) and thus generate a rudimental mABCC1 protein not detectable with the MRPr1 antibody. However, earlier studies have shown that such shortened ABCC1 proteins (the longest possible protein here would be devoid of the first 327 aa) lack proper sorting to the plasma membrane and are dysfunctional (Bakos et al., 2000; Bakos et al., 1998; Westlake et al., 2005; Yang et al., 2007). To prove functional ABCC1 expression in *hABCC1*$^{flx/flx}$ mice, as well as the lack thereof in *hABCC1*$^{-/-}$ mice, we utilized *in vivo* PET imaging.

6-bromo-7-[^{11}C]methylpurine has been introduced as a PET tracer to measure ABCC1 transport activity in the brain and lungs of mice (Okamura et al., 2009; Okamura et al., 2013). In the brain, 6-bromo-7-[^{11}C]methylpurine is converted in parenchymal cells (e.g. astrocytes) by glutathione-*S*-transferases into its glutathione conjugate S-(6-(7-[^{11}C]methylpurinyl))glutathione. The glutathione conjugate is then effluxed from parenchymal cells by ABCC1 followed by clearance across the blood-brain barrier by other anionic transporters (SLC22A8 and ABCC4) (Okamura et al., 2009; Okamura et al., 2018). Previous work has shown that *Abcc1*$^{-/-}$ mice possess an approximately 9-fold reduced $k_{elimination,brain}$ as compared with wild-type mice, supporting that transport by mABCC1 is the rate-limiting step in the elimination of 6-bromo-7-[^{11}C]methylpurine-derived radioactivity from the mouse brain (Okamura et al., 2009; Zoufal et al., 2019). In addition, *in vitro* transport experiments have demonstrated that the glutathione conjugate of 6-bromo-7-methylpurine is also a substrate of hABCC1 (Okamura et al., 2007). In the lungs, ABCC1 is expressed in the basolateral membrane of pulmonary epithelial cell types (airway epithelial cells, alveolar type 2 and type 1 cells) (Nickel et al., 2016). 6-bromo-7-[^{11}C]methylpurine PET revealed pronounced reductions in $k_{elimination,lung}$ in *Abcc1*$^{-/-}$ mice versus wild-type mice (Okamura et al., 2013; Zoufal et al., 2019). These great reductions in $k_{elimination,brain}$ and $k_{elimination,lung}$ in *Abcc1*$^{-/-}$ versus wild-type mice indicated absence of transporter redundancy for radiolabeled glutathione conjugate efflux in the cell membranes of brain parenchymal and pulmonary epithelial cells. Hence, the most likely explanation for similar clearance kinetics of radioactivity from brain and lungs in *hABCC1*$^{flx/flx}$ mice as compared with wild-type mice (Fig. 6A-D) is the replacement of endogenous mABCC1 transport activity by hABCC1 transport activity. In *hABCC1*$^{flx/flx}$ lungs, radioactivity clearance kinetics were nearly identical to those in wild-type mice (Figure 6B, F). In the brain, the radioactivity elimination was significantly higher in *hABCC1*$^{flx/flx}$ animals when compared to wild-type mouse brains (Figure 6A, E). These PET imaging data correlate well with the determined protein expression levels (Figure 4). Our results furthermore clearly show that *hABCC1*$^{-/-}$ mice are indeed fully deficient of ABCC1 transport activity. Interestingly, initial uptake of radioactivity in brain and lungs appeared to be lower in *hABCC1*$^{-/-}$ mice as compared with *hABCC1*$^{flx/flx}$ mice (Figure 6C, D). The initial concentrations of radioactivity in the brain and the lungs reflected unconverted 6-bromo-7-[^{11}C]methylpurine, which is believed to distribute to tissues *via* passive diffusion. One possible

Molecular Pharmacology Fast Forward. Published on June 12, 2019 as DOI: 10.1124/mol.119.115824
This article has not been copyedited and formatted. The final version may differ from this version.

explanation for the observed differences in initial tissue uptake of radioactivity could be differences in organ blood flow.

As expected, we also did not observe any overt phenotypical difference between *hABCC1*$^{flx/flx}$, *hABCC1*$^{-/-}$ and wild-type C57BL/6J mice while breeding or daily handling (Wijnholds et al., 1997). In combination with the large variety of commercially available organ and cell-type specific Cre-recombinase-expressing mouse lines, this model will allow researchers to apply *in vivo* experimental setups which have so far not been possible. For instance, it may become possible to reveal the effect of, e.g. ABCC1 knockout in capillary endothelia of the blood-brain barrier on drug distribution to the brain, the treatment of brain tumors or its effect on amyloid-beta pathology in Alzheimer's disease mouse models.

In summary, our data revealed a performance of the *hABCC1*$^{flx/flx}$ mice with regard to protein expression and function. Thus, we conclude that we have successfully achieved our goal of developing an *Abcc1* humanized mouse model with knockout capabilities.

Acknowledgments

We thank Thomas Filip, Michael Sauberer, Johann Stanek and Mathilde Löbsch for their invaluable help during the PET imaging sessions. We thank Wolfgang Härtig and his coworkers for technical support.

The establishment of the mice was financially supported by Immungenetics AG (Rostock, Germany). The mice are available to researchers at non-profit organizations without restrictions against a one-time contribution in order to help maintaining the strain.

The work of J.P. was financed by the following grants: Deutsche Forschungsgemeinschaft/ Germany (DFG PA930/9, PA930/12); Wirtschaftsministerium Sachsen-Anhalt/ Germany (EFRE ZS/2016/05/78617), the Leibniz Association (Leibniz-Wettbewerb SAW-2015-IPB-2); Latvian Council of Science/ Latvia (lzp-2018/1-0275); HelseSØ/ Norway (2016062, 2019054, 2019055); Norsk forskningsrådet/ Norway (251290 FRIMEDBIO, 260786 PROP-AD); Horizon 2020/ European Union (643417 (PROP-AD)).

The work of O.L. and T.W. was financed by the Austrian Science Fund (FWF) (grant number: I 1609-B24 to O.L.), and the Lower Austria Corporation for Research and Education (NFB) (grant number: LS14-008 to T. W.)

PROP-AD is an EU Joint Programme - Neurodegenerative Disease Research (JPND) project. The project is supported through the following funding organizations under the aegis of JPND - www.jpnd.eu (AKA

#301228 – Finland, BMBF #01ED1605- Germany, CSO-MOH #30000-12631 - Israel, NFR #260786 - Norway, SRC #2015-06795 - Sweden). This project has received funding from the European Union's Horizon 2020 research and innovation program under grant agreement #643417 (JPco-fuND).

Conflict of interest

The corresponding author is shareholder of Immungenetics AG.

Contributions

Participated in research design: Krohn, Langer, Pahnke

Conducted experiments: Krohn, Zoufal, Mairinger, Wanek, Paarmann, Brüning, Eiriz, Brackhan

Performed data analysis: Krohn, Zoufal, Mairinger, Wanek, Paarmann, Brüning, Eiriz, Brackhan

Wrote or contributed to the writing of the manuscript: Krohn, Langer, Pahnke

Molecular Pharmacology Fast Forward. Published on June 12, 2019 as DOI: 10.1124/mol.119.115824
This article has not been copyedited and formatted. The final version may differ from this version.

Figures

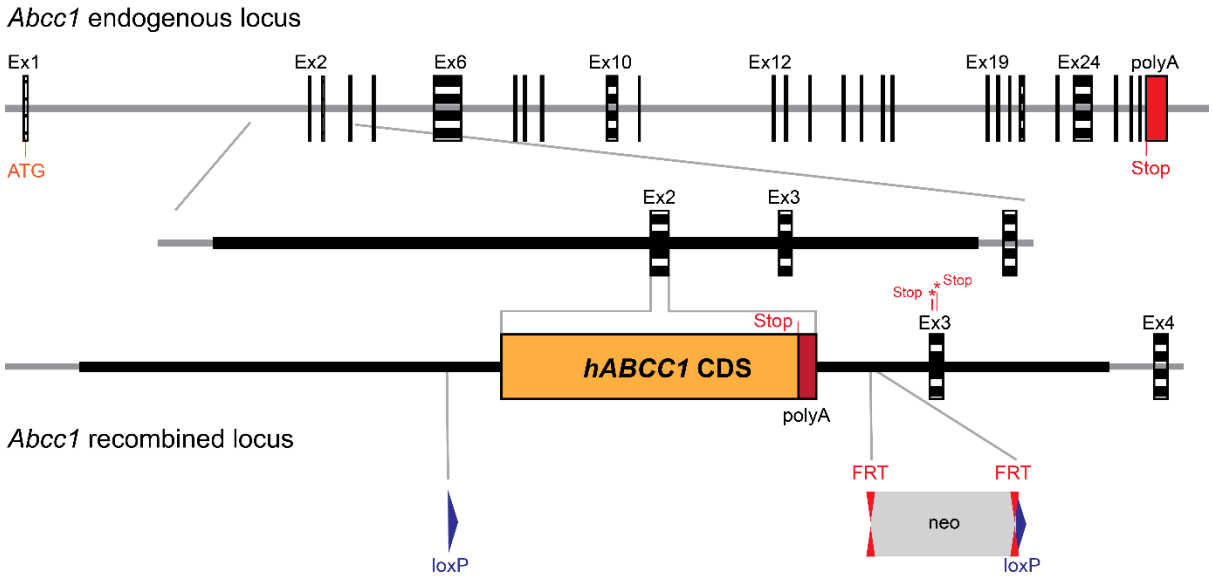

Figure 1. Targeting vector schematics and targeting strategy. Organization of the mouse *Abcc1* gene containing 28 exons (striped rectangles) is shown in the top row. Below, the targeted region encompassing exons 2 and 3 is magnified. The targeting construct was designed to replace exon 2 with the human *ABCC1* CDS (indicated by the gray lines). Long (upstream of exon 2) and short (downstream of exon 2) homology arms of the targeting vector are indicated as a black, solid line. They include loxP sites (blue triangles) and a Neomycin resistance cassette flanked by flippase recognition target sequences (FRT). Newly introduced stop-codons are indicated in exon 3.

Molecular Pharmacology Fast Forward. Published on June 12, 2019 as DOI: 10.1124/mol.119.115824
This article has not been copyedited and formatted. The final version may differ from this version.

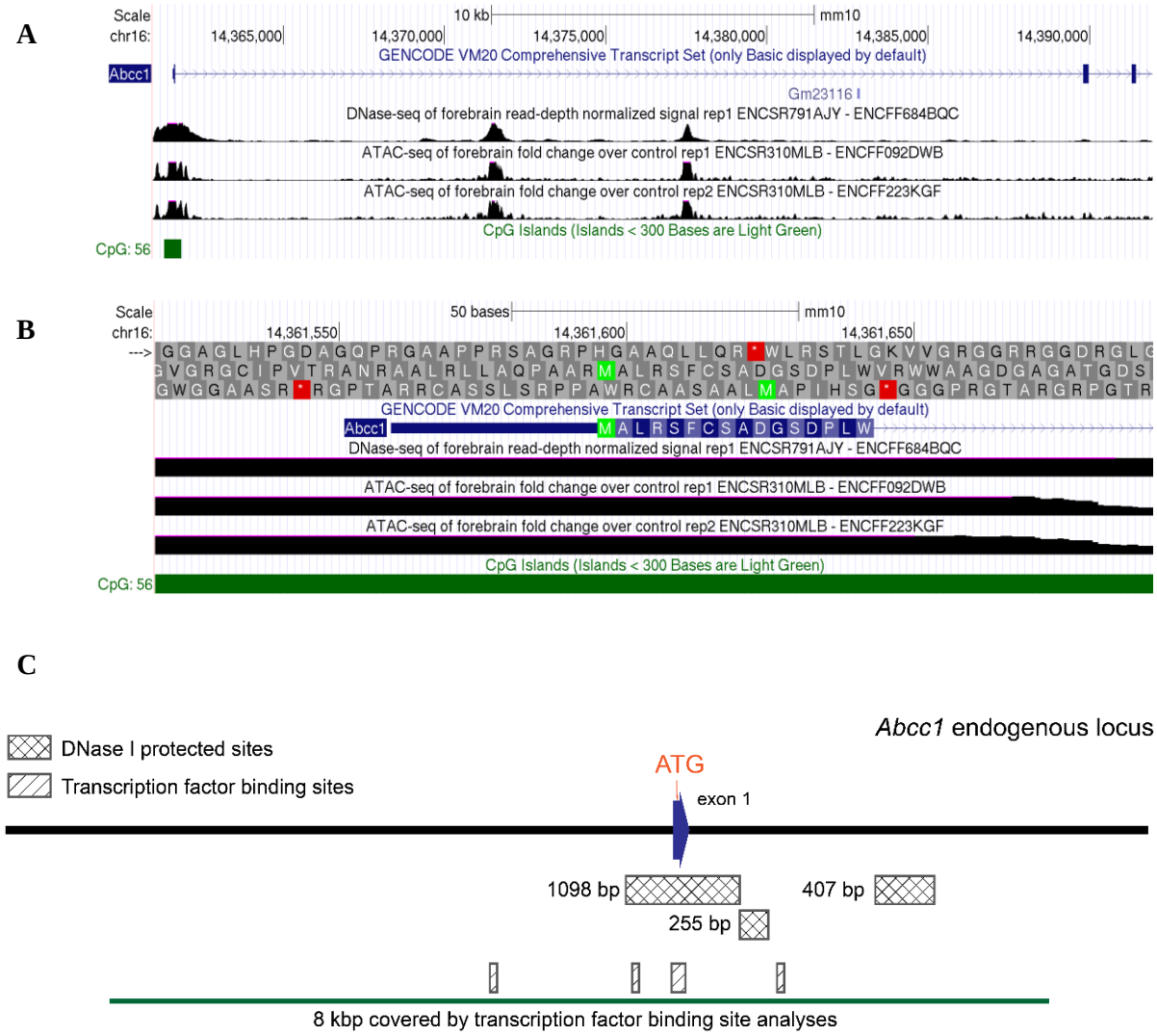

Figure 2. Schematic overview of potential regulatory elements.

Overview of DNase-seq and ATAC-seq data as well as location of CpG islands in the region within the first 3 exons (A, blue boxes) of the *Abcc1* gene. In B, a zoom into exon 1 is depicted. Pictures have been generated using UCSC genome browser (genome.ucsc.edu). C) Three DNase I protected sites and four conserved transcription factor binding sites were identified in the vicinity and within exon 1 of *Abcc1* in an in-house analysis by genOway®. Signals from all analyses indicate relevance of exon 1 and potentially intron 1 for regulation of *Abcc1* gene expression. In contrast, no such indicators are found around exons 2 and 3.

Molecular Pharmacology Fast Forward. Published on June 12, 2019 as DOI: 10.1124/mol.119.115824
This article has not been copyedited and formatted. The final version may differ from this version.

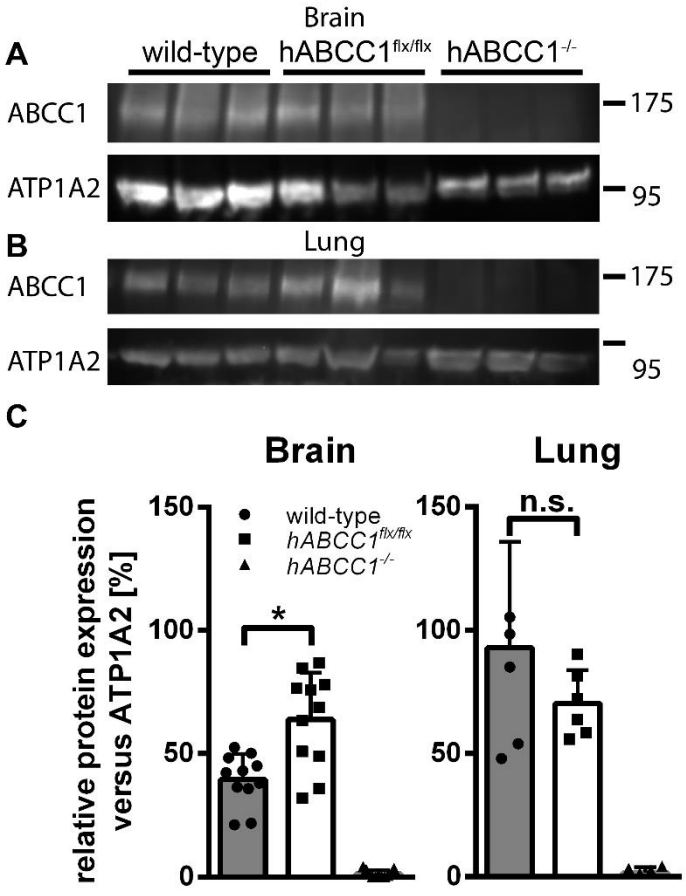

Fig. 3. Protein expression analysis. Representative Western blots (A, B) and quantitative analyses for ABCC1 protein expression (C) are shown for brain and lung tissue, respectively. Without having knowledge about the affinities of the MRPr1 antibody towards the human ABCC1 and mouse ABCC1 epitope, respectively (differs at epitope-position 1), ABCC1 protein expression in *hABCC1*$^{flx/flx}$ brains (n=6f/5m, white bar) appears significantly more abundant than in wild-type brains (n=5f/6m, grey bar) (A, C). In lung tissue, no significant difference between wild-type (n=2f/3m, grey bar) and *hABCC1*$^{flx/flx}$ mice (n=4f/2m, white bar) was detected (B, C). No significant expression of ABCC1 protein could be detected in *hABCC1*$^{-/-}$ brains (n=6f/5m) and lungs (n=2f/3m) (#). ATP1A2 raw signal values are reported in Supplementary table 3. Within each organ, one-way ANOVA of wild-type ABCC1 expression vs. all other groups was used, followed by Dunnett correction for multiple comparison. * $p<0.05$; error bars = SD.

Molecular Pharmacology Fast Forward. Published on June 12, 2019 as DOI: 10.1124/mol.119.115824
This article has not been copyedited and formatted. The final version may differ from this version.

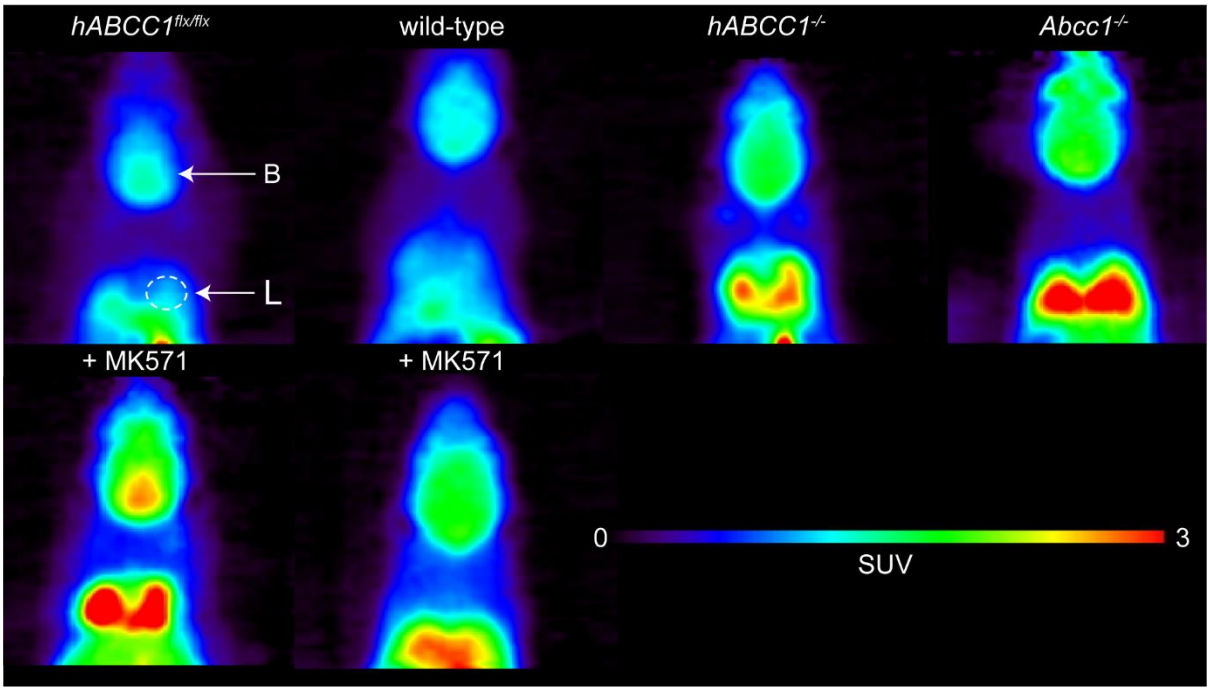

Figure 4. PET imaging of brain ABCC1 transport activity. Representative coronal PET images (0 - 90 min) of *hABCC1*$^{flx/flx}$, wild-type, *hABCC1*$^{-/-}$ and *Abcc1*$^{-/-}$ mice pre-treated with vehicle or MK571 (300 mg/kg, *i.p.*) at 30 min before the PET scan. Anatomic regions are labelled with arrows: B - brain, L - right lung. All images are scaled to the same intensity (0 - 3 standardized uptake value, SUV).

Molecular Pharmacology Fast Forward. Published on June 12, 2019 as DOI: 10.1124/mol.119.115824
This article has not been copyedited and formatted. The final version may differ from this version.

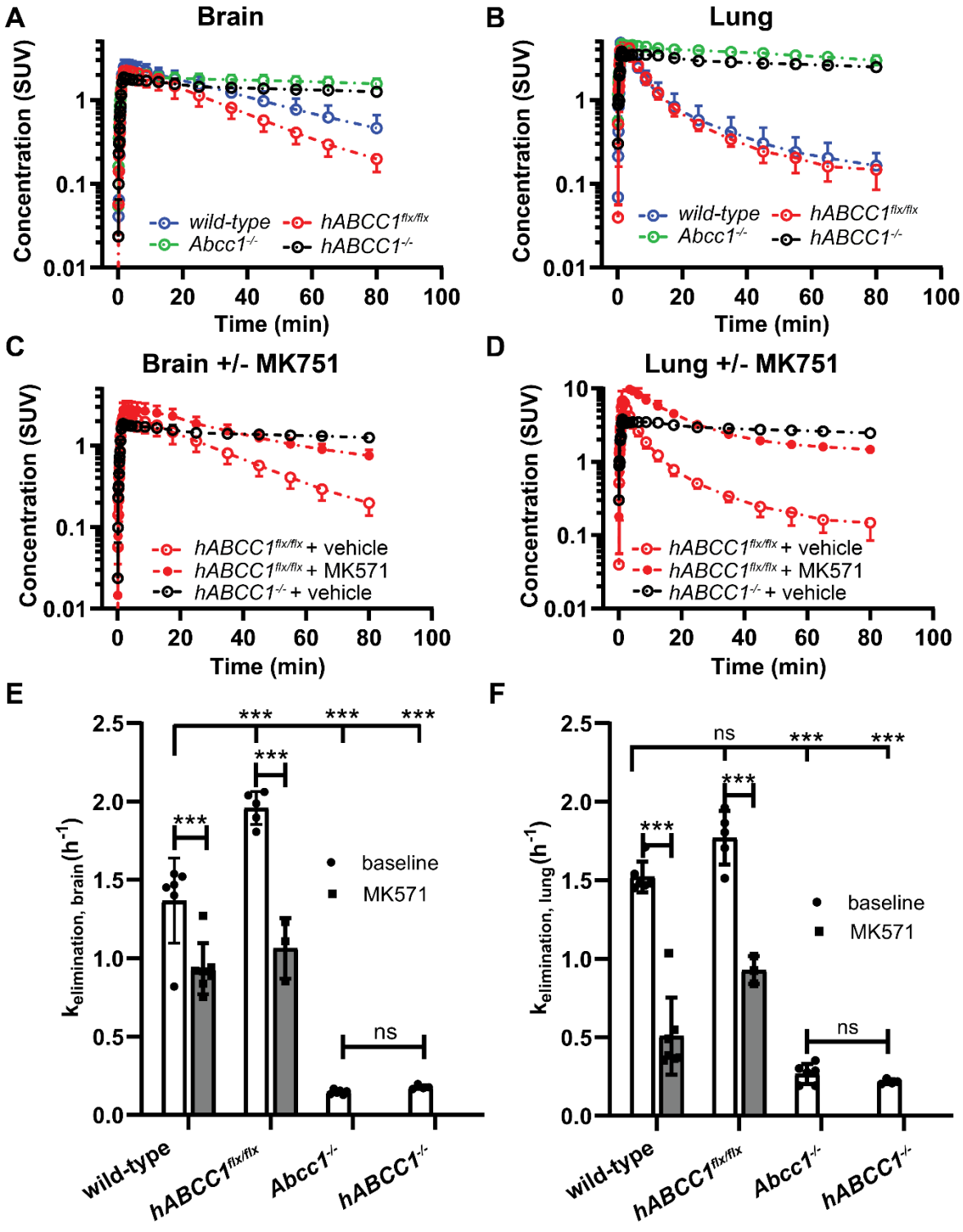

Figure 5. Quantification of brain and lung PET imaging. Concentration-time curves (mean standardized uptake value, SUV± SD) in brain (A) and right lung (B) of wild-type (n=6, females), *hABCC1*$^{flx/flx}$ (n=5, females), *Abcc1*$^{-/-}$ (n=6, females) and *hABCC1*$^{-/-}$ (n=4, females) mice. Concentration-

Molecular Pharmacology Fast Forward. Published on June 12, 2019 as DOI: 10.1124/mol.119.115824
This article has not been copyedited and formatted. The final version may differ from this version.

time curves in brain (C) and right lung (D) of *hABCC1*$^{flx/flx}$ mice pre-treated with vehicle or MK571 (300 mg/kg, *i.p.*) 30 min before PET (for comparison curves in *hABCC1*$^{-/-}$ are also shown). $K_{elimination}$ values (mean h^{-1} ± SD) of radioactivity from brain (E) and right lung (F) of wild-type, *hABCC1*$^{flx/flx}$, *Abcc1*$^{-/-}$ and *ABCC1*$^{-/-}$ mice with vehicle (white bars) or MK571 (grey bars) pre-treatment. *** $p<0.001$, one-way ANOVA followed by Tukey's multiple comparison test. Error bars = SD.

Molecular Pharmacology Fast Forward. Published on June 12, 2019 as DOI: 10.1124/mol.119.115824
This article has not been copyedited and formatted. The final version may differ from this version.

References

Alisi A, Cho WC, Locatelli F and Fruci D (2013) Multidrug resistance and cancer stem cells in neuroblastoma and hepatoblastoma. *Int J Mol Sci* **14**(12): 24706-24725.

Bakos E, Evers R, Calenda G, Tusnady GE, Szakacs G, Varadi A and Sarkadi B (2000) Characterization of the amino-terminal regions in the human multidrug resistance protein (MRP1). *J Cell Sci* **113 Pt 24**(24): 4451-4461.

Bakos E, Evers R, Szakacs G, Tusnady GE, Welker E, Szabo K, de Haas M, van Deemter L, Borst P, Varadi A and Sarkadi B (1998) Functional multidrug resistance protein (MRP1) lacking the N-terminal transmembrane domain. *J Biol Chem* **273**(48): 32167-32175.

Beedholm-Ebsen R, van de Wetering K, Hardlei T, Nexo E, Borst P and Moestrup SK (2010) Identification of multidrug resistance protein 1 (MRP1/ABCC1) as a molecular gate for cellular export of cobalamin. *Blood* **115**(8): 1632-1639.

Cartwright TA, Campos CR, Cannon RE and Miller DS (2013) Mrp1 is essential for sphingolipid signaling to p-glycoprotein in mouse blood-brain and blood-spinal cord barriers. *J Cereb Blood Flow Metab* **33**(3): 381-388.

Chen Q, Yang Y, Liu Y, Han B and Zhang JT (2002) Cytoplasmic retraction of the amino terminus of human multidrug resistance protein 1. *Biochemistry* **41**(29): 9052-9062.

Chihara D, Westin JR, Oki Y, Ahmed MA, Do B, Fayad LE, Hagemeister FB, Romaguera JE, Fanale MA, Lee HJ, Turturro F, Samaniego F, Neelapu SS, Rodriguez MA, Fowler NH, Wang M, Davis RE and Nastoupil LJ (2016) Management strategies and outcomes for very elderly patients with diffuse large B-cell lymphoma. *Cancer* **122**(20): 3145-3151.

Choo EF and Salphati L (2018) Leveraging Humanized Animal Models to Understand Human Drug Disposition: Opportunities, Challenges, and Future Directions. *Clin Pharmacol Ther* **103**(2): 188-192.

Citti A, Boldrini R, Inserra A, Alisi A, Pessolano R, Mastronuzzi A, Zin A, De Sio L, Rosolen A, Locatelli F and Fruci D (2012) Expression of multidrug resistance-associated proteins in paediatric soft tissue sarcomas before and after chemotherapy. *Int J Oncol* **41**(1): 117-124.

Cole SP (2014) Multidrug resistance protein 1 (MRP1, ABCC1), a "multitasking" ATP-binding cassette (ABC) transporter. *J Biol Chem* **289**(45): 30880-30888.

Crowder SW, Balikov DA, Hwang YS and Sung HJ (2014) Cancer Stem Cells under Hypoxia as a Chemoresistance Factor in Breast and Brain. *Curr Pathobiol Rep* **2**(1): 33-40.

Dallas S, Salphati L, Gomez-Zepeda D, Wanek T, Chen L, Chu X, Kunta J, Mezler M, Menet MC, Chasseigneaux S, Decleves X, Langer O, Pierre E, DiLoreto K, Hoft C, Laplanche L, Pang J, Pereira T, Andonian C, Simic D, Rode A, Yabut J, Zhang X and Scheer N (2016) Generation and Characterization of a Breast Cancer Resistance Protein Humanized Mouse Model. *Mol Pharmacol* **89**(5): 492-504.

de Sousa Abreu R, Penalva LO, Marcotte EM and Vogel C (2009) Global signatures of protein and mRNA expression levels. *Mol Biosyst* **5**(12): 1512-1526.

Devoy A, Bunton-Stasyshyn RK, Tybulewicz VL, Smith AJ and Fisher EM (2011) Genomically humanized mice: technologies and promises. *Nature reviews Genetics* **13**(1): 14-20.

Gao M, Yamazaki M, Loe DW, Westlake CJ, Grant CE, Cole SP and Deeley RG (1998) Multidrug resistance protein. Identification of regions required for active transport of leukotriene C4. *J Biol Chem* **273**(17): 10733-10740.

Giordano SH, Lin YL, Kuo YF, Hortobagyi GN and Goodwin JS (2012) Decline in the use of anthracyclines for breast cancer. *J Clin Oncol* **30**(18): 2232-2239.

Haber M, Smith J, Bordow SB, Flemming C, Cohn SL, London WB, Marshall GM and Norris MD (2006) Association of high-level MRP1 expression with poor clinical outcome in a large prospective study of primary neuroblastoma. *J Clin Oncol* **24**(10): 1546-1553.

Hipfner DR, Almquist KC, Leslie EM, Gerlach JH, Grant CE, Deeley RG and Cole SP (1997) Membrane topology of the multidrug resistance protein (MRP). A study of glycosylation-site mutants reveals an extracytosolic NH2 terminus. *J Biol Chem* **272**(38): 23623-23630.

Hipfner DR, Gao M, Scheffer G, Scheper RJ, Deeley RG and Cole SP (1998) Epitope mapping of monoclonal antibodies specific for the 190-kDa multidrug resistance protein (MRP). *Br J Cancer* **78**(9): 1134-1140.

Hofrichter J, Krohn M, Schumacher T, Lange C, Feistel B, Walbroel B, Heinze HJ, Crockett S, Sharbel TF and Pahnke J (2013) Reduced Alzheimer's disease pathology by St. John's Wort treatment is independent of hyperforin and facilitated by ABCC1 and microglia activation in mice. *Curr Alzheimer Res* **10**(10): 1057-1069.

Huang Z, Cheng L, Guryanova OA, Wu Q and Bao S (2010) Cancer stem cells in glioblastoma--molecular signaling and therapeutic targeting. *Protein Cell* **1**(7): 638-655.

International Transporter C, Giacomini KM, Huang SM, Tweedie DJ, Benet LZ, Brouwer KL, Chu X, Dahlin A, Evers R, Fischer V, Hillgren KM, Hoffmaster KA, Ishikawa T, Keppler D, Kim RB, Lee CA, Niemi M, Polli JW, Sugiyama Y, Swaan PW, Ware JA, Wright SH, Yee SW, Zamek-Gliszczynski MJ and Zhang L (2010) Membrane transporters in drug development. *Nature reviews Drug discovery* **9**(3): 215-236.

Islam MO, Kanemura Y, Tajria J, Mori H, Kobayashi S, Shofuda T, Miyake J, Hara M, Yamasaki M and Okano H (2005) Characterization of ABC transporter ABCB1 expressed in human neural stem/progenitor cells. *FEBS Lett* **579**(17): 3473-3480.

Jedlitschky G, Leier I, Buchholz U, Barnouin K, Kurz G and Keppler D (1996) Transport of glutathione, glucuronate, and sulfate conjugates by the MRP gene-encoded conjugate export pump. *Cancer Res* **56**(5): 988-994.

Krohn M, Bracke A, Avchalumov Y, Schumacher T, Hofrichter J, Paarmann K, Frohlich C, Lange C, Bruning T, von Bohlen Und Halbach O and Pahnke J (2015) Accumulation of murine amyloid-beta mimics early Alzheimer's disease. *Brain* **138**(Pt 8): 2370-2382.

Krohn M, Lange C, Hofrichter J, Scheffler K, Stenzel J, Steffen J, Schumacher T, Bruning T, Plath AS, Alfen F, Schmidt A, Winter F, Rateitschak K, Wree A, Gsponer J, Walker LC and Pahnke J (2011) Cerebral amyloid-beta proteostasis is regulated by the membrane transport protein ABCC1 in mice. *J Clin Invest* **121**(10): 3924-3931.

Krohn M, Wanek T, Menet MC, Noack A, Decleves X, Langer O, Loscher W and Pahnke J (2018) Humanization of the Blood-Brain Barrier Transporter ABCB1 in Mice Disrupts Genomic Locus - Lessons from Three Unsuccessful Approaches. *Eur J Microbiol Immunol (Bp)* **8**(3): 78-86.

Kurz EU, Cole SP and Deeley RG (2001) Identification of DNA-protein interactions in the 5' flanking and 5' untranslated regions of the human multidrug resistance protein (MRP1) gene: evaluation of a putative antioxidant response element/AP-1 binding site. *Biochem Biophys Res Commun* **285**(4): 981-990.

Leier I, Jedlitschky G, Buchholz U and Keppler D (1994) Characterization of the ATP-dependent leukotriene C4 export carrier in mastocytoma cells. *Eur J Biochem* **220**(2): 599-606.

Leslie EM, Letourneau IJ, Deeley RG and Cole SP (2003) Functional and structural consequences of cysteine substitutions in the NH2 proximal region of the human multidrug resistance protein 1 (MRP1/ABCC1). *Biochemistry* **42**(18): 5214-5224.

Liu B, Li LJ, Gong X, Zhang W, Zhang H and Zhao L (2018) Co-expression of ATP binding cassette transporters is associated with poor prognosis in acute myeloid leukemia. *Oncol Lett* **15**(5): 6671-6677.

Loening AM and Gambhir SS (2003) AMIDE: a free software tool for multimodality medical image analysis. *Mol Imaging* **2**(3): 131-137.

Maier T, Guell M and Serrano L (2009) Correlation of mRNA and protein in complex biological samples. *FEBS Lett* **583**(24): 3966-3973.

Martin-Broto J, Gutierrez AM, Ramos RF, Lopez-Guerrero JA, Ferrari S, Stacchiotti S, Picci P, Calabuig S, Collini P, Gambarotti M, Bague S, Dei Tos AP, Palassini E, Luna P, Cruz J, Cubedo R,

Martinez-Trufero J, Poveda A, Casali PG, Fernandez-Serra A, Lopez-Pousa A and Gronchi A (2014) MRP1 overexpression determines poor prognosis in prospectively treated patients with localized high-risk soft tissue sarcoma of limbs and trunk wall: an ISG/GEIS study. *Mol Cancer Ther* **13**(1): 249-259.

McGowan JV, Chung R, Maulik A, Piotrowska I, Walker JM and Yellon DM (2017) Anthracycline Chemotherapy and Cardiotoxicity. *Cardiovasc Drugs Ther* **31**(1): 63-75.

Muller M, Meijer C, Zaman GJ, Borst P, Scheper RJ, Mulder NH, de Vries EG and Jansen PL (1994) Overexpression of the gene encoding the multidrug resistance-associated protein results in increased ATP-dependent glutathione S-conjugate transport. *Proc Natl Acad Sci U S A* **91**(26): 13033-13037.

Muredda M, Nunoya K, Burtch-Wright RA, Kurz EU, Cole SP and Deeley RG (2003) Cloning and Characterization of the Murine and Rat mrp1 Promoter Regions. *Mol Pharmacol* **64**(5): 1259-1269.

Nabhan C, Byrtek M, Rai A, Dawson K, Zhou X, Link BK, Friedberg JW, Zelenetz AD, Maurer MJ, Cerhan JR and Flowers CR (2015) Disease characteristics, treatment patterns, prognosis, outcomes and lymphoma-related mortality in elderly follicular lymphoma in the United States. *Br J Haematol* **170**(1): 85-95.

Nickel S, Clerkin CG, Selo MA and Ehrhardt C (2016) Transport mechanisms at the pulmonary mucosa: implications for drug delivery. *Expert opinion on drug delivery* **13**(5): 667-690.

Noguchi K, Katayama K and Sugimoto Y (2014) Human ABC transporter ABCG2/BCRP expression in chemoresistance: basic and clinical perspectives for molecular cancer therapeutics. *Pharmgenomics Pers Med* **7**: 53-64.

Okamura T, Kikuchi T, Fukushi K, Arano Y and Irie T (2007) A novel noninvasive method for assessing glutathione-conjugate efflux systems in the brain. *Bioorg Med Chem* **15**(9): 3127-3133.

Okamura T, Kikuchi T, Okada M, Toramatsu C, Fukushi K, Takei M and Irie T (2009) Noninvasive and quantitative assessment of the function of multidrug resistance-associated protein 1 in the living brain. *J Cereb Blood Flow Metab* **29**(3): 504-511.

Okamura T, Kikuchi T, Okada M, Wakizaka H and Zhang MR (2013) Imaging of activity of multidrug resistance-associated protein 1 in the lungs. *Am J Respir Cell Mol Biol* **49**(3): 335-340.

Okamura T, Okada M, Kikuchi T, Wakizaka H and Zhang MR (2018) Mechanisms of glutathione-conjugate efflux from the brain into blood: Involvement of multiple transporters in the course. *J Cereb Blood Flow Metab*: 271678X18808399.

Pahnke J, Frohlich C, Krohn M, Schumacher T and Paarmann K (2013) Impaired mitochondrial energy production and ABC transporter function-A crucial interconnection in dementing proteopathies of the brain. *Mech Ageing Dev* **134**(10): 506-515.

Pascal LE, True LD, Campbell DS, Deutsch EW, Risk M, Coleman IM, Eichner LJ, Nelson PS and Liu AY (2008) Correlation of mRNA and protein levels: cell type-specific gene expression of cluster designation antigens in the prostate. *BMC Genomics* **9**: 246.

Peignan L, Garrido W, Segura R, Melo R, Rojas D, Carcamo JG, San Martin R and Quezada C (2011) Combined use of anticancer drugs and an inhibitor of multiple drug resistance-associated protein-1 increases sensitivity and decreases survival of glioblastoma multiforme cells in vitro. *Neurochem Res* **36**(8): 1397-1406.

Sadiq MW, Uchida Y, Hoshi Y, Tachikawa M, Terasaki T and Hammarlund-Udenaes M (2015) Validation of a P-Glycoprotein (P-gp) Humanized Mouse Model by Integrating Selective Absolute Quantification of Human MDR1, Mouse Mdr1a and Mdr1b Protein Expressions with In Vivo Functional Analysis for Blood-Brain Barrier Transport. *PloS one* **10**(5): e0118638.

Schumacher T, Krohn M, Hofrichter J, Lange C, Stenzel J, Steffen J, Dunkelmann T, Paarmann K, Frohlich C, Uecker A, Plath AS, Sommer A, Bruning T, Heinze HJ and Pahnke J (2012) ABC transporters B1, C1 and G2 differentially regulate neuroregeneration in mice. *PloS one* **7**(4): e35613.

Smith LA, Cornelius VR, Plummer CJ, Levitt G, Verrill M, Canney P and Jones A (2010) Cardiotoxicity of anthracycline agents for the treatment of cancer: systematic review and meta-analysis of randomised controlled trials. *BMC Cancer* **10**: 337.

Stride BD, Grant CE, Loe DW, Hipfner DR, Cole SP and Deeley RG (1997) Pharmacological characterization of the murine and human orthologs of multidrug-resistance protein in transfected human embryonic kidney cells. *Mol Pharmacol* **52**(3): 344-353.

Theodoulou FL and Kerr ID (2015) ABC transporter research: going strong 40 years on. *Biochem Soc Trans* **43**(5): 1033-1040.

Tivnan A, Zakaria Z, O'Leary C, Kogel D, Pokorny JL, Sarkaria JN and Prehn JH (2015) Inhibition of multidrug resistance protein 1 (MRP1) improves chemotherapy drug response in primary and recurrent glioblastoma multiforme. *Front Neurosci* **9**: 218.

Torres A, Vargas Y, Uribe D, Jaramillo C, Gleisner A, Salazar-Onfray F, Lopez MN, Melo R, Oyarzun C, San Martin R and Quezada C (2016) Adenosine A3 receptor elicits chemoresistance mediated by multiple resistance-associated protein-1 in human glioblastoma stem-like cells. *Oncotarget* **7**(41): 67373-67386.

van der Kolk DM, de Vries EG, van Putten WJ, Verdonck LF, Ossenkoppele GJ, Verhoef GE and Vellenga E (2000) P-glycoprotein and multidrug resistance protein activities in relation to treatment outcome in acute myeloid leukemia. *Clin Cancer Res* **6**(8): 3205-3214.

Vogel C and Marcotte EM (2012) Insights into the regulation of protein abundance from proteomic and transcriptomic analyses. *Nature reviews Genetics* **13**(4): 227-232.

Westlake CJ, Cole SP and Deeley RG (2005) Role of the NH2-terminal membrane spanning domain of multidrug resistance protein 1/ABCC1 in protein processing and trafficking. *Mol Biol Cell* **16**(5): 2483-2492.

Wijaya J, Fukuda Y and Schuetz JD (2017) Obstacles to Brain Tumor Therapy: Key ABC Transporters. *Int J Mol Sci* **18**(12).

Wijnholds J, Evers R, van Leusden MR, Mol CA, Zaman GJ, Mayer U, Beijnen JH, van der Valk M, Krimpenfort P and Borst P (1997) Increased sensitivity to anticancer drugs and decreased inflammatory response in mice lacking the multidrug resistance-associated protein. *Nat Med* **3**(11): 1275-1279.

Winter SS, Ricci J, Luo L, Lovato DM, Khawaja HM, Serna-Gallegos T, Debassige N and Larson RS (2013) ATP Binding Cassette C1 (ABCC1/MRP1)-mediated drug efflux contributes to disease progression in T-lineage acute lymphoblastic leukemia. *Health (Irvine Calif)* **5**(5A).

Yamasaki Y, Kobayashi K, Okuya F, Kajitani N, Kazuki K, Abe S, Takehara S, Ito S, Ogata S, Uemura T, Ohtsuki S, Minegishi G, Akita H, Chiba K, Oshimura M and Kazuki Y (2018) Characterization of P-Glycoprotein Humanized Mice Generated by Chromosome Engineering Technology: Its Utility for Prediction of Drug Distribution to the Brain in Humans. *Drug Metab Dispos* **46**(11): 1756-1766.

Yang Y, Liu Y, Dong Z, Xu J, Peng H, Liu Z and Zhang JT (2007) Regulation of function by dimerization through the amino-terminal membrane-spanning domain of human ABCC1/MRP1. *J Biol Chem* **282**(12): 8821-8830.

Zhang DW, Cole SP and Deeley RG (2001) Identification of an amino acid residue in multidrug resistance protein 1 critical for conferring resistance to anthracyclines. *J Biol Chem* **276**(16): 13231-13239.

Zoufal V, Mairinger S, Krohn M, Wanek T, Filip T, Sauberer M, Stanek J, Traxl A, Schuetz JD, Kuntner C, Pahnke J and Langer O (2019) Influence of Multidrug Resistance-Associated Proteins on the Excretion of the ABCC1 Imaging Probe 6-Bromo-7-[(11)C]Methylpurine in Mice. *Mol Imaging Biol* **21**(2): 306-316.